

PAPER • OPEN ACCESS

Low-dimensional manifold of actin polymerization dynamics

To cite this article: Carlos Floyd *et al* 2017 *New J. Phys.* **19** 125012

View the [article online](#) for updates and enhancements.

You may also like

- [Pulling-force generation by ensembles of polymerizing actin filaments](#)
F Motahari and A E Carlsson

- [How capping protein enhances actin filament growth and nucleation on biomimetic beads](#)
Ruizhe Wang and Anders E Carlsson

- [Interplay between membrane tension and the actin cytoskeleton determines shape changes](#)
Camille Simon, Valentina Caorsi, Clément Campillo et al.

New Journal of Physics

The open access journal at the forefront of physics

Deutsche Physikalische Gesellschaft 

IOP Institute of Physics

Published in partnership
with: Deutsche Physikalische
Gesellschaft and the Institute
of Physics



OPEN ACCESS

RECEIVED
14 August 2017

REVISED
18 October 2017

ACCEPTED FOR PUBLICATION
26 October 2017

PUBLISHED
18 December 2017

Original content from this
work may be used under
the terms of the Creative
Commons Attribution 3.0
licence.

Any further distribution of
this work must maintain
attribution to the
author(s) and the title of
the work, journal citation
and DOI.



PAPER

Low-dimensional manifold of actin polymerization dynamics

Carlos Floyd¹ , Christopher Jarzynski^{1,2,3,4}  and Garegin Papoian^{1,2,3,5} 

¹ Biophysics Program, University of Maryland, College Park, MD 20742 United States of America

² Department of Chemistry and Biochemistry, University of Maryland, College Park, MD 20742 United States of America

³ Institute for Physical Science and Technology, University of Maryland, College Park, MD 20742 United States of America

⁴ Department of Physics, University of Maryland, College Park, MD 20742 United States of America

⁵ Author to whom any correspondence should be addressed.

E-mail: cjarzyns@umd.edu and gpapoian@umd.edu

Keywords: actin, polymerization dynamics, cytoskeleton, Drazin inverse, polymer physics, diffusion map, dynamical manifolds

Supplementary material for this article is available [online](#)

Abstract

Actin filaments are critical components of the eukaryotic cytoskeleton, playing important roles in a number of cellular functions, such as cell migration, organelle transport, and mechanosensation. They are helical polymers with a well-defined polarity, composed of globular subunits that bind nucleotides in one of three hydrolysis states (ATP, ADP-Pi, or ADP). Mean-field models of the dynamics of actin polymerization have succeeded in, among other things, determining the nucleotide profile of an average filament and resolving the mechanisms of accessory proteins. However, these models require numerical solution of a high-dimensional system of nonlinear ordinary differential equations. By truncating a set of recursion equations, the Brooks–Carlsson (BC) model reduces dimensionality to 11, but it still remains nonlinear and does not admit an analytical solution, hence, significantly hindering understanding of its resulting dynamics. In this work, by taking advantage of the fast timescales of the hydrolysis states of the filament tips, we propose two model reduction schemes: the quasi steady-state approximation model is five-dimensional and nonlinear, whereas the constant tip (CT) model is five-dimensional and linear, resulting from the approximation that the tip states are not dynamic variables. We provide an exact solution of the CT model and use it to shed light on the dynamical behaviors of the full BC model, highlighting the relative ordering of the timescales of various collective processes, and explaining some unusual dependence of the steady-state behavior on initial conditions.

1. Introduction

Actin filaments are an integral part of the cytoskeleton of eukaryotes and are involved in functions such as controlling cell shape, cell motility, organelle redistribution, and mechanical coupling with the cellular environment. These filaments are formed of globular subunits which polymerize in a nonequilibrium process that *in vivo* is modulated by an array of accessory proteins. They are helical and polar, with distinct plus ('barbed') and minus ('pointed') ends at which subunits have different rates of association and dissociation [1]. Hydrolysis of cellular adenosine triphosphate (ATP) leads to filament 'treadmilling', in which there are equal and opposite rates of polymerization at the barbed and pointed ends of the filaments, which drives the polymerization process away from equilibrium and allows actin networks to be responsive to cellular signals on relatively fast timescales [2–4]. Each actin subunit molecule is bound to a nucleotide, which can be in one of several hydrolysis states: ATP, adenosine diphosphate (ADP), or an intermediate state ADP-Pi, in which ADP is still bound to a hydrolyzed inorganic phosphate molecule. Release of inorganic phosphate by ADP-Pi converts it to ADP [5]. The hydrolysis state of the bound nucleotide has dramatic effects on the kinetic polymerization and depolymerization rate constants of the globular subunit [6]. In addition, these hydrolysis states affect the binding affinity of accessory proteins as well as structural properties such as filament persistence length [7, 8]. Thus it is of interest to be able to predict the hydrolysis state of the nucleotide bound to each actin subunit in a filament, or at least the fraction of actin subunits bound to nucleotides in a certain hydrolysis state.

Over several decades a variety of models describing actin polymerization dynamics have been put forward, and these models have evolved alongside the growth of experimental knowledge about the nature of actin. Some early models tracked the number of filaments with a certain degree of polymerization under different assumptions about the filament polarity, geometry, and the cooperativity of polymerization, among other factors [9–14]. Polymerization and depolymerization rate constants for ATP and ADP-bound actin were measured for the first time in 1986 [6]. A subset of more recent models have investigated aspects such as the effects of accessory proteins on actin polymerization by tracking the time-varying concentrations of actin subunits distinguished by their polymerization state and by the hydrolysis state of the nucleotide they are bound to. A variable is assigned to the concentration of each species and of complexes between certain species, and equations of motion in terms of mean-field kinetic rate constants are written for each. In this context, ‘mean-field’ refers to the assumption that the solution of actin subunits and accessory proteins is homogeneous and obeys mass-action kinetics. The resulting coupled ordinary differential equations (ODEs) are solved numerically, and the effects of varying parameters such as reservoir ATP/ADP disequilibrium, total filament concentration, fraction of capped plus ends, free actin concentration, and profilin concentration are investigated [15, 16]. One point of contention is whether transitions between hydrolysis states of polymerized subunits occur in a random fashion, in which hydrolysis states of a subunit’s neighbors do not affect the hydrolysis rate of that subunit, or in a vectorial fashion, in which an ATP-bound subunit will only hydrolyze ATP if its neighbor towards the minus end is ADP-Pi bound, leading to a contiguous ATP-bound cap at the plus end. Recent models suggest that the truth is in the middle, such that coupling exists in ATP cleavage rates between neighboring polymerized subunits, but not such that the process is truly vectorial [17, 18]. Most mean-field models make the assumption of random ATP hydrolysis for simplicity.

An important disadvantage of such mean-field models aimed at resolving the roles of accessory proteins is that their level of detail inhibits analytical solutions to the time courses and, hence, obscures deeper insights into dynamical behaviors of these systems. While this approach has successfully allowed modelers to, for example, rule out certain mechanisms of profilin’s action on critical concentrations [19], one might ask what is the simplest such model that reproduces time courses from more detailed models. This is the aim of the present work. The model reduction here is based on a 2009 model by Brooks and Carlsson (BC) [20], which presents a system of differential equations that admits only numerical solution but does not include extra detail by accounting for accessory proteins. It is useful for predicting the process of polymerization when a pool of subunits are added to an initial concentration of seed filaments, and is sufficiently simple to be incorporated into larger-scale cellular models without too much additional computational cost.

In this work, we report on two successive reduction schemes of the 11-dimensional BC model: a quasi-steady-state approximation (QSSA) that leverages fast dynamics of the filament tips, leading to a five-dimensional system of ODEs, and a subsequent linearization approximation. The latter equations admit an analytical solution whose implications we investigate, revealing interesting features of the actin polymerization process projected on the slow dynamical manifold. Our analytical model reduction approaches show excellent agreement with the results obtained from stochastic simulations of the full BC model and also when compared with diffusion mapping analyses of stochastic trajectories.

2. Methods

2.1. Brooks–Carlsson model

The BC model of actin polymerization is an 11-dimensional system of ODEs tracking the concentrations of non-tip actin subunits in different states as well as the concentrations of filament tip subunits in different states [20]. It is assumed that the number concentration of filaments N remains constant, implying an absence of filament nucleation, splitting, or joining. Additionally, the total concentration of actin subunits M is assumed to remain constant, such that actin subunits are not created or destroyed in any reaction. Since there are typically many actin subunits belonging to a given actin filament, we have $N \ll M$. All species are assumed to be well-mixed and in large enough quantities to be treated effectively via a mean-field description. In other words, the size of the stochastic fluctuations is negligible compared to the concentrations of the species. Unpolymerized (globular) actin subunits are referred to as G-actin, while polymerized (filamentous) actin subunits are referred to as F-actin. Actin filaments are helical, but they are more easily modeled as linear chains, which is a realistic approximation if one assumes that the reaction propensities of a given F-actin subunit are determined only by the state of the nucleotide bound by that subunit and not by the subunit’s neighbors. Such a chain is displayed in figure 1, along with some of the reactions allowing interconversion between subunit types. The variables representing the concentrations of these actin species are superscripted by the hydrolysis state of the bound nucleotide (for what follows we refer more simply to a subunit being in a certain hydrolysis state as opposed to the nucleotide attached to a subunit as being in that state). The hydrolysis states are ATP, ADP-Pi, and ADP,

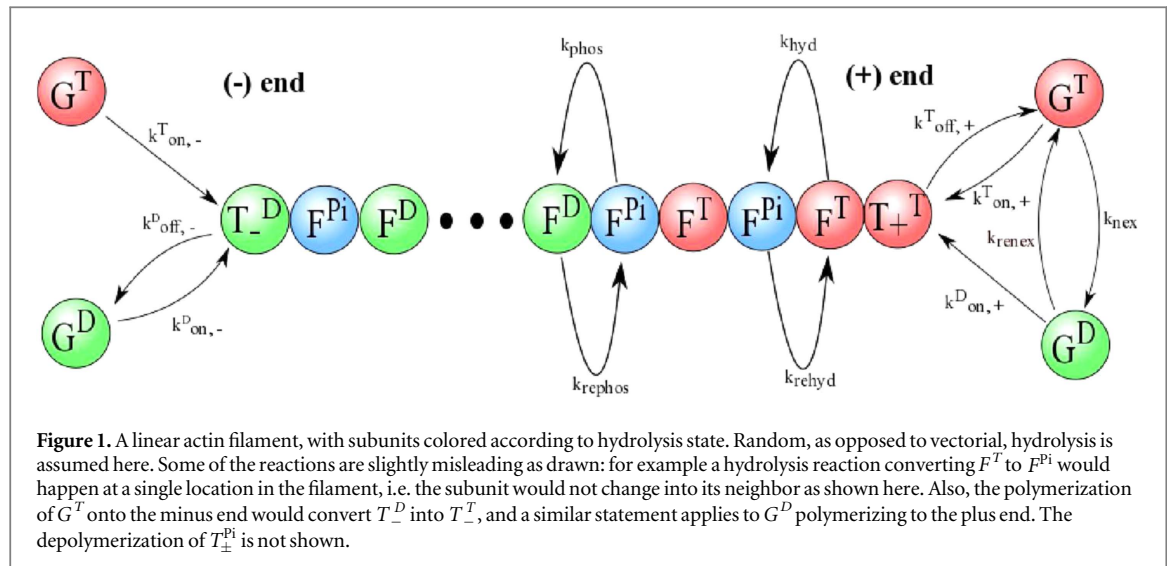


Figure 1. A linear actin filament, with subunits colored according to hydrolysis state. Random, as opposed to vectorial, hydrolysis is assumed here. Some of the reactions are slightly misleading as drawn: for example a hydrolysis reaction converting F^T to F^{Pi} would happen at a single location in the filament, i.e. the subunit would not change into its neighbor as shown here. Also, the polymerization of G^T onto the minus end would convert T^D into T^T , and a similar statement applies to G^D polymerizing to the plus end. The depolymerization of T^D is not shown.

denoted T , Pi , and D , respectively. The tip subunits are denoted T and are further subscripted according to which tip they are on. Thus, for example, the concentration of tip subunits at the plus end bound to ADP-Pi is denoted T_+^{Pi} . Because inorganic phosphate rapidly dissociates from G-actin, G^{Pi} is taken to be 0 and is not tracked. With the 3 hydrolysis states of each of the 2 tips, the 3 states of the F-actin and the 2 states of G-actin, the number of tracked variables is 11.

The different subunit types interconvert through chemical reactions. These reactions can be classified as polymerization/depolymerization reactions which change G actin to F actin and vice versa, or as reactions in which the hydrolysis state of the subunit changes. The evolution of the concentrations of a given tip subunit hydrolysis states in principle depends on the hydrolysis state of the subunit adjacent to the tip, which itself depends on the hydrolysis state of the next subunit in the filament, and so on. Every subunit in the filament then requires explicit tracking, causing the dimensionality of the model to be roughly equal to the degree of polymerization of a filament, which typically contains hundreds of subunits. The major accomplishment of the BC model is to truncate this set of recursion equations by assuming that the hydrolysis state of the subunit adjacent to the tip depends only on the hydrolysis state of the tip subunit. Using the results of stochastic simulations of a more complete model, they write empirical equations to capture these relationships, and in doing so they close off an 11-dimensional subset of the original hundreds of equations. They find close agreement between their truncated model and the full stochastic simulation over a wide and realistic range of parameters.

The equations of motion for the 11 variables in the BC model can be written as a nonlinear system of ODEs:

$$\dot{\mathbf{x}} = \mathbf{f}(\mathbf{x}), \quad (1)$$

where \mathbf{x} is a vector of the concentrations of the 11 species, and \mathbf{f} is a nonlinear vector-valued function of \mathbf{x} . This system of equations must be solved numerically, but the results match well with simulations that accurately model experimental data [21]. The steady-state vector \mathbf{x}^{ss} satisfying $\mathbf{f}(\mathbf{x}^{ss}) = \mathbf{0}$ is unique for given values of N and M and under the condition that all concentrations be real and non-negative, and it is attracting. We give more details of the BC model in appendix A, where we list the 11 ODEs.

A separation of timescales exists between the dynamics of the non-tip subunit states and those of tip subunit states: the latter evolve much more rapidly than the former. Thus we partition the vector \mathbf{x} into slow and fast variables: $\mathbf{x}_s \equiv (G^T, G^D, F^T, F^{Pi}, F^D)^T$, $\mathbf{x}_f \equiv (T_+^T, T_+^{Pi}, T_+^D, T_-^T, T_-^{Pi}, T_-^D)^T$, where the subscripts ‘s’ and ‘f’ refer to ‘slow’ and ‘fast’. Terms of comparable magnitude appear in the equations of motion for both \mathbf{x}_f and \mathbf{x}_s , but the elements in \mathbf{x}_f are typically much smaller than those in \mathbf{x}_s because $N \ll M$, so \mathbf{x}_f reaches equilibrium more rapidly since the distance to equilibrium is not as large as it is for \mathbf{x}_s . To see the separation timescales concretely, we refer the reader to the end of section 3.1, where we show the spectrum of the Jacobian matrix of the BC model evaluated at steady-state. With the new collective variables \mathbf{x}_s and \mathbf{x}_f , equation (1) can be usefully rewritten as follows:

$$\dot{\mathbf{x}}_s = \mathbf{A}\mathbf{x}_s + \mathbf{B}\mathbf{x}_f, \quad (2)$$

$$\dot{\mathbf{x}}_f = \mathbf{h}(\mathbf{x}_s, \mathbf{x}_f), \quad (3)$$

where \mathbf{A} and \mathbf{B} are matrices whose off-diagonal elements are combinations of kinetic rate constants and whose columns sum to zero due to conservation of actin, and \mathbf{h} is a nonlinear vector-valued function containing terms that are up to cubic products of variables.

The BC model provides a computationally accessible model of the dynamics of actin polymerization, however we might ask for several other features in such a model. We ask that it: (1) be low-dimensional, (2) capture the interesting and important timescales, and (3) be exactly solvable. To meet these goals, we make the decision to track only the vector \mathbf{x}_s explicitly. If we were to track the concentration of the tip subunit states, i.e. the elements in \mathbf{x}_f , we would automatically increase the dimensionality of the model, and we will discuss reasons why we may assume that the tip subunits are evolving in such a way that keeping track of them explicitly is unnecessary. We make two approximations for how to treat \mathbf{x}_f in equation (2), first utilizing the fact that a separation of timescale exists between the dynamics of \mathbf{x}_f and \mathbf{x}_s , and then utilizing the fact that $|\mathbf{Bx}_f| \ll |\mathbf{Ax}_s|$ except when the system is near its steady-state, at which point these terms have comparable magnitudes. This second approximation follows since \mathbf{x}_f contains terms up to $\mathcal{O}(N)$ and \mathbf{x}_s contains terms up to $\mathcal{O}(M)$.

It is also possible to demonstrate that a low-dimensional description of the slow dynamics is a valid approximation through the use of diffusion mapping on a stochastically generated data set based on the BC model. We describe this analysis in supporting information 1 which is available online at stacks.iop.org/NJP/19/125012/mmedia.

2.2. Quasi-steady-state approximation

The QSSA relies on a separation of timescales between fast and slow variables. This separation allows one to assume that the fast variables \mathbf{x}_f are always in equilibrium with respect to the slow variables \mathbf{x}_s , and therefore that the values of the slow variables determine the values of the fast variables at any moment. We can imagine that \mathbf{x}_f is effectively being ‘dragged around’ by the values of the elements in \mathbf{x}_s . So, we can solve for functions $\mathbf{x}_f^{\text{eq}}(\mathbf{x}_s)$ relating the quasi-equilibrated fast variables in terms of the slow variables by imagining holding \mathbf{x}_s fixed and finding the equilibrium values of \mathbf{x}_f . This amounts to the condition $\mathbf{h}(\mathbf{x}_f^{\text{eq}}; \mathbf{x}_s) = \mathbf{0}$. The functions $\mathbf{x}_f^{\text{eq}}(\mathbf{x}_s)$ are then substituted in the equations of motion for the slow variables giving the closed system of equations

$$\dot{\mathbf{x}}_s = \mathbf{Ax}_s + \mathbf{Bx}_f^{\text{eq}}(\mathbf{x}_s). \quad (4)$$

This subsystem is lower-dimensional, though it is nonlinear since $\mathbf{x}_f^{\text{eq}}(\mathbf{x}_s)$ is nonlinear, and it describes the evolution of the system on the slow timescales.

In the BC model, the condition $\mathbf{h}(\mathbf{x}_f^{\text{eq}}; \mathbf{x}_s) = \mathbf{0}$ implies the following algebraic systems of equations (see appendix A):

$$\begin{aligned} \frac{dT_{\pm}^T}{dt} &= 0, \\ \frac{dT_{\pm}^{\text{Pi}}}{dt} &= 0, \\ \frac{dT_{\pm}^D}{dt} &= 0. \end{aligned} \quad (5)$$

Only four of these six equations are linearly independent due to the conservation of number of plus and minus end filament tips, so we use the following supplementary equations to find a solution of the combined systems of equations:

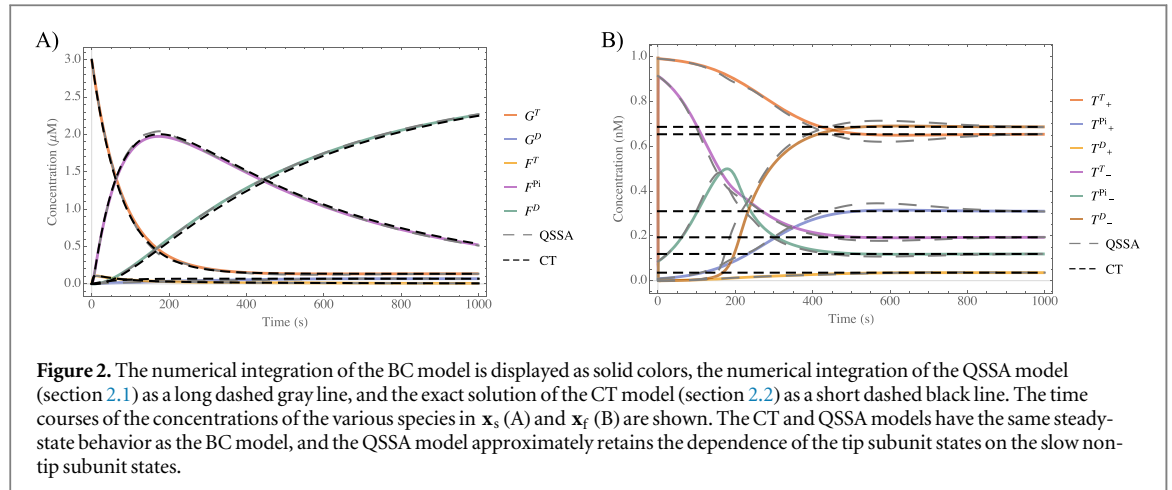
$$T_{\pm}^T + T_{\pm}^{\text{Pi}} + T_{\pm}^D = N. \quad (6)$$

System of equations (5), (6) can be solved numerically resulting in tabulated functions of the forms $T_{\pm}^T(G^T, G^D)$, $T_{\pm}^{\text{Pi}}(G^T, G^D)$, and $T_{\pm}^D(G^T, G^D)$. These functions do not depend on F^T , F^{Pi} , and F^D because these variables do not enter into the function \mathbf{h} . Subsequently, the nonlinear (slow) system described by equation (4) is numerically integrated. Figure 2 displays a comparison of the QSSA approximation to the original 11-dimensional BC model.

This approximation succeeds in reducing the dimensionality of the model to 5. We note, however, that the dynamics of this model lie on a four-dimensional submanifold of the full five-dimensional manifold due to the fact that \mathbf{A} and \mathbf{B} are both singular, corresponding to conservation of actin. This model also captures the interesting timescales describing polymerization events and dynamics of the hydrolysis states of F and G actin, while it neglects the fast dynamics corresponding to events taking place at the tips. However the model is still nonlinear and analytically unsolvable, so we propose an alternative model reduction scheme.

2.3. Constant tip approximation

In addition to having sufficiently fast dynamics as to be effectively described as in quasi-equilibrium with respect to \mathbf{x}_s , the vector \mathbf{x}_f is also small in magnitude compared to \mathbf{x}_s , and this fact can be utilized to drastically simplify the QSSA model. Although the tip dynamics are fast, one can profitably assume that the concentration of filament tip subunit states, that is, the elements in \mathbf{x}_f , are constant in time. We refer to this assumption as the constant tip (CT) approximation. Certainly this assumption is not realistic since the tips have fast dynamics, but the effect of this error on the equations of motion of the other actin species is small in the regime where the



number concentration of filaments is much smaller than the total amount of actin in the system, i.e. when $N \ll M$, or if the tip subunit states quickly attain their limiting values. This assumption allows the model to be reduced to a five-dimensional linear system of equations that can be solved analytically. The procedure is to replace the dynamical variables T_j^i by constants $N\Gamma_j^i$, chosen such that the steady-state of the CT model coincides with the steady-state of the BC model. We define Γ_j^i as the fraction of the filament tips at the j (plus or minus) end that are in the $i(T, P_i, D)$ hydrolysis state. These constants determine the rate of depolymerization reactions, and replacing the variables T_j^i with them causes the term \mathbf{Bx}_f to be a constant source and sink term in equation (2), which as a result becomes linear.

The steady-states of the BC and CT models will be the same if

$$\begin{aligned} N\Gamma_{\pm}^T &= \lim_{t \rightarrow \infty} T_{\pm}^T(t), \\ N\Gamma_{\pm}^{Pi} &= \lim_{t \rightarrow \infty} T_{\pm}^{Pi}(t), \\ N\Gamma_{\pm}^D &= \lim_{t \rightarrow \infty} T_{\pm}^D(t). \end{aligned} \quad (7)$$

In other words, the CT subunit state fractions in the CT model should be chosen as the steady-state values of the tip subunit state fractions in the BC model. As a result, only the approach to steady-state will be different between the two models. These limiting values can be found by numerically solving the algebraic system of equations

$$\begin{aligned} \mathbf{f}(\mathbf{x}^{ss}) &= 0, \\ T_{\pm}^T + T_{\pm}^{Pi} + T_{\pm}^D &= N, \\ G^T + G^D + F^T + F^{Pi} + F^D &= M, \end{aligned} \quad (8)$$

where \mathbf{x}^{ss} is the 11-dimensional steady-state vector of concentrations in the BC model, and taking the real non-negative solution. Equation (8) determines the values of Γ_j^i which will be unique for a given N and M .

We define

$$\mathbf{b} \equiv \mathbf{Bx}_f^{ss}, \quad (9)$$

where \mathbf{x}_f^{ss} contains the constants $N\Gamma_j^i$ instead of the variables T_j^i . The equation of motion for \mathbf{x}_s is

$$\dot{\mathbf{x}}_s = \mathbf{Ax}_s + \mathbf{b}, \quad (10)$$

where

$$\mathbf{A} = \begin{pmatrix} -a - b & c & 0 & 0 & 0 \\ b & -c - d & 0 & 0 & 0 \\ a & 0 & -e & f & 0 \\ 0 & 0 & e & -f - g & h \\ 0 & d & 0 & g & -h \end{pmatrix}, \quad (11)$$

$$\mathbf{b} = \begin{pmatrix} i \\ j + k \\ -i \\ -k \\ -j \end{pmatrix} \quad (12)$$

with

$$\begin{aligned}
 a &= N(k_{\text{on},+}^T + k_{\text{off},+}^T) & g &= k_{\text{phos}} \\
 b &= k_{\text{nex}} & h &= k_{\text{rephos}} \\
 c &= k_{\text{renex}} & i &= N(\Gamma_+^T k_{\text{off},+}^T + \Gamma_-^T k_{\text{off},-}^T) \\
 d &= N(k_{\text{on},+}^D + k_{\text{off},+}^D) & j &= N(\Gamma_+^D k_{\text{off},+}^D + \Gamma_-^D k_{\text{off},-}^D) \\
 e &= k_{\text{hyd}} & k &= N(\Gamma_+^{\text{Pi}} k_{\text{off},+}^{\text{Pi}} + \Gamma_-^{\text{Pi}} k_{\text{off},-}^{\text{Pi}}) \\
 f &= k_{\text{rehyd}}
 \end{aligned} \tag{13}$$

Equation (10) is a linear system of differential equations which can be solved exactly. One point of difficulty in solving this system is that the columns of \mathbf{A} sum to zero due to conservation of actin, causing \mathbf{A} to be singular. In chemical reaction network theory, one often has such systems with linear conservation laws. If the system is linear, with only first order or pseudo-first order reactions, then such a singular system can be solved cleanly by a method using the Drazin inverse \mathbf{A}^D of the matrix \mathbf{A} . We believe that this method has certain advantages over other approaches to solving singular systems of differential equations. If \mathbf{A} has Jordan decomposition

$$\mathbf{A} = \mathbf{V} \begin{pmatrix} J_1 & 0 \\ 0 & J_0 \end{pmatrix} \mathbf{V}^{-1}, \tag{14}$$

where J_1 and J_0 correspond to the non-zero and zero eigenvalues respectively, then

$$\mathbf{A}^D = \mathbf{V} \begin{pmatrix} J_1^{-1} & 0 \\ 0 & 0 \end{pmatrix} \mathbf{V}^{-1}. \tag{15}$$

In supporting information 2 in the supplementary material we go over the details of solving equation (10) as well as the advantages of this method [22]. The solution is

$$\mathbf{x}_s = (-\mathbf{A}^D + e^{\mathbf{A}t} \mathbf{G}) \mathbf{b}. \tag{16}$$

The matrix

$$\mathbf{G} = \frac{1}{|\mathbf{b}|^2} \mathbf{x}_s(0) \mathbf{b}^\top + \mathbf{A}^D \tag{17}$$

encodes information about the initial conditions $\mathbf{x}_s(0)$.

3. Results

3.1. Eigenvalues of A

Perhaps the most important benefit of an exactly solvable model is the ability to formally determine the eigenvalues governing the linear dynamics. These eigenvalues characterize the relaxation times of the components of a perturbation from equilibrium, in the basis of the eigenvectors. The expressions for the eigenvalues thus shed light on the timescales that describe the different chemical processes. In our modeling we have included the reverses of kinetically dominant forward reactions, and we have set the rate constants of these reactions to be equal to something on the order of the corresponding forward reaction rate constants multiplied by a small parameter ϵ . Thus $b = \epsilon b^*$, where $b^* \sim c$, $f = \epsilon f^*$, where $f^* \sim e$, and $h = \epsilon h^*$, where $h^* \sim g$. By writing reverse rate constants this way, we can Taylor expand the expressions for the eigenvalues around the point $\epsilon = 0$ to simplify the result. Doing so to first order in ϵ , we have

$$\lambda_1 = 0, \tag{18}$$

$$\begin{aligned}
 \lambda_2 &= \frac{1}{2}(-a - \epsilon b^* - c - d + \sqrt{(a - d + \epsilon b^* - c)^2 + 4\epsilon b^* c}) \\
 &\approx -c - d + \frac{b^* c}{a - c - d} \epsilon.
 \end{aligned} \tag{19}$$

$$\begin{aligned}
 \lambda_3 &= \frac{1}{2}(-a - \epsilon b^* - c - d - \sqrt{(a - d + \epsilon b^* - c)^2 + 4\epsilon b^* c}) \\
 &\approx -a - \frac{b^*(a - d)}{a - c - d} \epsilon,
 \end{aligned} \tag{20}$$

$$\begin{aligned}
 \lambda_4 &= \frac{1}{2}(-e - \epsilon f^* - g - \epsilon h^* + \sqrt{(e - g + \epsilon f^* - \epsilon h^*)^2 + 4\epsilon f^* g}) \\
 &\approx -g - \left(h^* - \frac{gf^*}{e - g} \right) \epsilon,
 \end{aligned} \tag{21}$$

$$\begin{aligned}\lambda_5 &= \frac{1}{2}(-e - \epsilon f^* - g - \epsilon h^* - \sqrt{(e - g + \epsilon f^* - \epsilon h^*)^2 + 4\epsilon f^* g}) \\ &\approx -e - \frac{\epsilon f^*}{e - g} \epsilon.\end{aligned}\quad (22)$$

The fact that the nonzero eigenvalues are negative implies the stability of the steady-state. These eigenvalues have no dependence on M , the total concentration of actin subunits, but they do depend on N , the number concentration of filaments, since this term appears in the expressions for a and d . For the parameterization used here and with $N = 1$ nM, the eigenvalues can be ordered by magnitude as follows:

$$|\lambda_5| > |\lambda_3| > |\lambda_2| > |\lambda_4| > |\lambda_1|. \quad (23)$$

Equations (18)–(22) are in terms of reaction rate constants and can be interpreted as representing certain collective subprocesses in the chemical system corresponding to combinations of those reactions. The ordering indicates the comparative rates of those subprocesses. We interpret the zeroth order terms of the eigenvalues as follows:

- $\lambda_1 = 0$ because actin subunits are conserved in this system, causing \mathbf{A} to be singular. Equivalently, one can say that the dynamics unfold on a four-dimensional submanifold of the five-dimensional manifold, and that this submanifold is determined by M .
- λ_2 represents the combination of the forward nucleotide exchange reaction ($G^D \rightarrow G^T$) and the polymerization of G^D . Both of these reactions convert G^D into another species, so this eigenvalue represents the subprocess of G^D depletion.
- λ_3 represents the polymerization of G^T .
- λ_4 represents the release of phosphate by F^{Pi} to form F^D .
- λ_5 represents the hydrolysis of ATP converting F^T to F^{Pi} .

Whether the magnitudes of these eigenvalues are increased or decreased due to the presence of reversible reactions (i.e. when $\epsilon > 0$) depends on the parameterization, since the sign of the first order terms depend on the comparative sizes of certain parameters.

In the full BC 11-dimensional model, one can numerically evaluate the Jacobian matrix of $\mathbf{f}(\mathbf{x})$ at steady-state,

$$\mathbf{J}^* \equiv \left. \frac{\partial \mathbf{f}}{\partial \mathbf{x}} \right|_{\mathbf{x}=\mathbf{x}^{ss}}. \quad (24)$$

We find that, for the same parameterization, the smallest four non-zero eigenvalues of \mathbf{J}^* are numerically equal to the non-zero eigenvalues of \mathbf{A} . This implies that the CT model has captured the slowest dynamics of the BC model by ignoring the processes involving the tip subunits. The main benefit of the CT approximation is that these slow linear dynamics can now be easily analyzed. These dynamics provide information about the polymerization process, the nucleotide composition of the filaments, and nucleotide exchange of globular actin. For most purposes, these aspects are of primary interest, and the processes at the tips are of lesser importance.

To quantitatively judge the separation of timescales of the BC model, we list the nonzero numerically evaluated eigenvalues of \mathbf{J}^* when $N = 1$ nM and $\epsilon = 0$, in decreasing magnitude ($-5.49, -1.41, -0.833, -0.393, -0.300, -0.0130, -0.0129, -0.002$). For comparison, we do the same with the eigenvalues of \mathbf{A} ($-0.300, -0.0130, -0.0129, -0.002$). While there is no large spectral gap, there is certainly a wide range of timescales, and it would suffice to even keep the smallest 3 non-zero eigenvalues. We later show how, by combining certain species, the dimensionality can be reduced to 3.

3.2. Steady-state concentrations

One might expect that if we increase the amount of actin subunits in the system by a different choice of initial conditions, the concentrations of the different species at steady-state would change. An interesting feature of this system is that this is true only for some species, and which species it is true for depends on whether or not we have included reversible reactions (if $\epsilon > 0$). Additionally, this can be shown to be true in both the CT model and the BC model. We demonstrate it first in the CT model.

We find the steady-state vector of concentrations \mathbf{x}_s^{ss} by taking the limit of equation (16) as $t \rightarrow \infty$,

$$\mathbf{x}_s^{ss} \equiv \lim_{t \rightarrow \infty} \mathbf{x}_s(t) = -\mathbf{A}^D \mathbf{b} + \mathbf{C} \mathbf{G} \mathbf{b}, \quad (25)$$

where

$$\mathbf{C} \equiv \lim_{t \rightarrow \infty} e^{\mathbf{A}t}. \quad (26)$$

We eigendecompose \mathbf{A} as \mathbf{UDV}^\dagger and use it in the expression for \mathbf{C} ,

$$\mathbf{C} = \mathbf{U} \lim_{t \rightarrow \infty} e^{\mathbf{D}t} \mathbf{V}^\dagger. \quad (27)$$

With the exception of λ_1 , which is zero, the eigenvalues of \mathbf{A} are negative, so we have

$$\begin{aligned} \mathbf{C} &= \mathbf{U} \text{diag}(1, 0, 0, 0, 0) \mathbf{V}^\dagger \\ &= \begin{pmatrix} 0 & 0 & 0 & 0 & 0 \\ 0 & 0 & 0 & 0 & 0 \\ \frac{fh}{eg} & 0 & 0 & 0 & 0 \\ \frac{h}{g} & 0 & 0 & 0 & 0 \\ 1 & 0 & 0 & 0 & 0 \end{pmatrix} \mathbf{V}^\dagger, \end{aligned} \quad (28)$$

where $\left(0, 0, \frac{fh}{eg}, \frac{h}{g}, 1\right)^\top$ is the eigenvector corresponding to λ_1 . Thus the top two rows of \mathbf{C} are zero, and the top four rows would be zero if we exclude reversible reactions. This is also true of the term $\mathbf{C}\mathbf{G}\mathbf{b}$. Now, the matrix \mathbf{G} is the only place where the initial conditions appear in equation (25). So if the top two rows $\mathbf{C}\mathbf{G}\mathbf{b}$ are zero, then the first two elements of \mathbf{x}_s^{ss} cannot have any dependence on initial conditions. In other words, G^D and G^T always reach the same concentrations at steady-state no matter what the initial concentrations of any of the species are. If we have no reversible reactions, the same is also true for the species F^T and F^{Pi} .

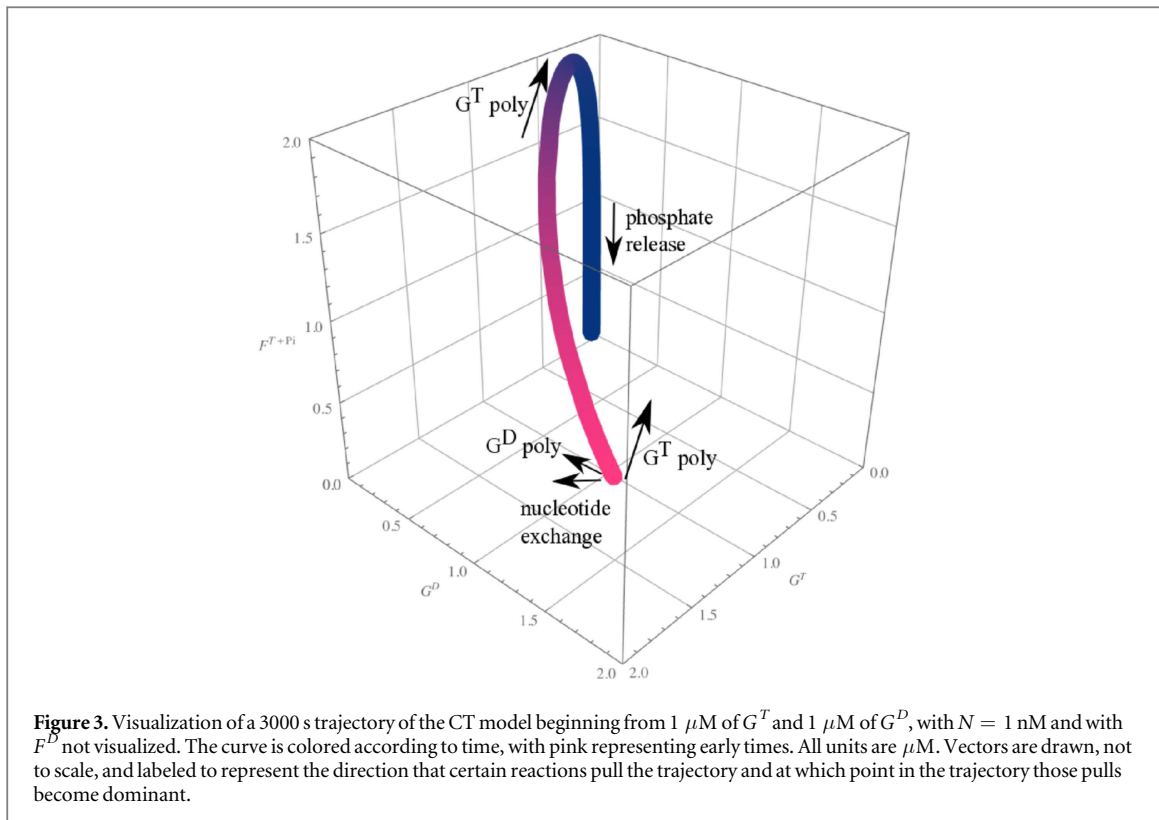
Consider the following thought experiment, assuming for simplicity $\epsilon = 0$. We start with some initial amount M of actin in any form and let the system come to steady-state. We then add an amount ΔM more actin to the system, in any form, and wait until the system has reached steady-state again. We would find that the only difference between the two steady-states is that the concentration of F^D had increased by ΔM . If $\epsilon > 0$, then we would find that the steady-state values of F^T and F^{Pi} , F^D had all increased, and the sum of these changes would be ΔM .

This lack of dependence of the steady-state concentrations of some species on M is not an artifact of the CT approximation; it is also the case in the BC model. It can not be shown to be true by taking the limit $t \rightarrow \infty$ as is the case here, but it can instead be shown by observing that a subset of the system of algebraic equations $\mathbf{f}(\mathbf{x}^{ss}) = 0$ is closed, and that a solution for the subset could be obtained without specifying M . This implies that the steady-state concentrations of the species represented by that solution have no dependence on M . We give the details of this argument in appendix B.

4. Discussion

We have argued that the dynamics of the polymerization of actin subunits into filaments can effectively be subdivided as follows: fast nonlinear dynamics govern the states of the filament tip subunits, and slow linear dynamics govern the change in polymerization and hydrolysis states of non-tip subunits. One cannot completely separate the tip subunit dynamics from the non-tip subunit dynamics because they are coupled; the tip subunit states depend on the concentrations of G^T and G^D through polymerization reactions, and the non-tip subunit states depend on the tip subunit states via depolymerization reactions. However, because of the typical size of N compared to M , the non-tip subunit states depend only comparatively weakly on the tip subunit states during most of a typical trajectory. We have shown two ways to approximate this coupling to achieve a significant reduction in dimensionality of the system. First, in the QSSA model, it is assumed that, on the slow timescale, the number of tips in a certain hydrolysis state depends only on G^T and G^D . This allows one to write a closed system of equations of motion of the non-tip subunits, describing evolution of the entire system on the slow five-dimensional submanifold of the full 11-dimensional space. This model is physically realistic and quite accurate because it preserves the dependence of the tip subunit states on the concentration of the non-tip subunits, however the resulting equations of motion are analytically intractable.

In the CT model, we make the seemingly unrealistic assumption that the tip subunits have no dependence on the non-tip subunits and in fact do not evolve at all, but remain fixed for all times at their steady-state values. In this sense we turn the tip subunit concentrations from variables into constants, and the equations of motion for the non-tip subunits become five-dimensional and linear with the depolymerization terms involving the tip subunits entering as a non-homogenous term \mathbf{b} . By choosing the fixed values of the tip subunits as the resting values, we ensure that the steady-states of the two models will be the same. The CT assumption is valid because of



the weak dependence of the non-tip subunit states on the tip subunit states. In other words, \mathbf{b} is comparatively small, and the discrepancy between trajectories of the CT and BC model due to \mathbf{b} not containing realistic values for all times is not pronounced. In exchange for the cost of this error, there is an important benefit, which is the ability to write symbolic expressions for the eigenvalues of the matrix \mathbf{A} . We note that these eigenvalues agree with the numerically calculated smallest nonzero eigenvalues of \mathbf{J}^* of the full 11-dimensional model, indicating that indeed the linear non-tip subunit dynamics are the slowest of all of the processes in the BC model. In addition, qualitative results about the nature of the dependence of the steady-state concentrations on the initial conditions agree for the full and reduced model. We have also shown dimensionality reduction to be possible by diffusion map analysis of a simulated trajectory of the BC model (supporting information 1). The results of this analysis indicate that fewer than 6 or 7 dimensions suffice to faithfully reproduce the polymerization dynamics.

Eigenvalue analysis of \mathbf{A} allows one to understand the timescales that govern the linear non-tip subunit dynamics as well as how these timescales depend on the parameters. These timescales approximately represent the following processes: depletion of G^D via polymerization and conversion to G^T , polymerization of G^T , hydrolysis of ATP converting F^T to F^{Pi} , and phosphate release converting F^{Pi} to F^D . As might be expected, the timescales involving polymerization depend on N , and their magnitude compared to that of the other timescales may change significantly. We have treated the presence of the reverses of some nearly irreversible reactions essentially as perturbations by regarding the rate constants of backward reactions as equal to the rate constant of the corresponding forward reaction multiplied by a small parameter ϵ . As shown above, the inclusion of these reactions introduce small corrections to the eigenvalues. These timescales allow one to understand a typical trajectory of the system. Such a trajectory can be visualized in three dimensions by combining multiple species into a single species and choosing to not to visualize a variable whose value is determined by the other three due to conservation of actin. In figure 3, we combine F^T and F^{Pi} together, since they have similar structural properties in the filament, and we do not visualize F^D . Thus we further reduce dimensionality to 4 (of which only 3 dimensions are independent) by neglecting the timescale corresponding to ATP hydrolysis, i.e. λ_5 . In the trajectory depicted, G^T and G^D are quickly made small via polymerization and nucleotide exchange reactions. The polymerization of G^T causes F^{T+Pi} to increase, and when G^T has become small, F^{T+Pi} converts to F^D via the slow process of phosphate release, and at the end, nearly all of the actin is in the form F^D .

5. Conclusion

The main results of this work are the elucidation of the degree to which not explicitly accounting for tip subunit state dynamics during actin polymerization is a passable assumption, and the resulting insight into the hierarchy

of processes involved in the slow linear dynamics of the non-tip subunit states. The CT model is overly simple but useful to understand basic features of the polymerization process. In other more detailed models, actin related proteins are incorporated either by introducing new variables representing the proteins and the protein-subunit complexes, or by including new parameters that multiply certain terms in the equations of motion [15, 16, 19]. These adaptations could be straightforwardly included in the modeling done here. Additionally, the effect of different concentrations of solvated ATP, ADP-Pi, and ADP could be investigated by changing the values of the pseudo-first order reaction rate constants, or even by regarding those reactions as second order and tracking the concentrations of the nucleotide species as separate variables. These modifications run counter to the goal here of model reduction, however. Different choices in modeling are of course suited to different purposes, and the choices made here address a desire to have a simple mental picture of an otherwise obscured and complex process.

Acknowledgments

We would like to thank Maria Cameron, for her helpful comments regarding the diffusion map analysis presented in this work, and Andrew Maven Smith, for his insights into the solution of the CT model, among other things. This work is supported by NSF CHE-136081 and NSF DMR-1506969.

Appendix A. Details of Brooks–Carlsson model

The BC model consists of the following set of 11 coupled ODEs:

$$\frac{dG^T}{dt} = k_{\text{off},+}^T T_+^T + k_{\text{off},-}^T T_-^T + k_{\text{nex}} G^D - k_{\text{renex}} G^T - G^T N (k_{\text{on},+}^T + k_{\text{on},-}^T), \quad (29)$$

$$\begin{aligned} \frac{dG^D}{dt} = & k_{\text{off},+}^D T_+^D + k_{\text{off},-}^D T_-^D + k_{\text{off},+}^{\text{Pi}} T_+^{\text{Pi}} + k_{\text{off},-}^{\text{Pi}} T_-^{\text{Pi}} + k_{\text{renex}} G^T - k_{\text{nex}} G^D \\ & - G^D N (k_{\text{on},+}^D + k_{\text{on},-}^D), \end{aligned} \quad (30)$$

$$\frac{dF^T}{dt} = G^T N (k_{\text{on},+}^T + k_{\text{on},-}^T) - k_{\text{off},+}^T T_+^T - k_{\text{off},-}^T T_-^T - k_{\text{hyd}} F^T + k_{\text{rehyd}} F^{\text{Pi}}, \quad (31)$$

$$\frac{dF^{\text{Pi}}}{dt} = k_{\text{hyd}} F^T - k_{\text{rehyd}} F^{\text{Pi}} - k_{\text{off},+}^{\text{Pi}} T_+^{\text{Pi}} - k_{\text{off},-}^{\text{Pi}} T_-^{\text{Pi}} - k_{\text{phos}} F^{\text{Pi}} + k_{\text{rephos}} F^D, \quad (32)$$

$$\frac{dF^D}{dt} = G^D N (k_{\text{on},+}^D + k_{\text{on},-}^D) + k_{\text{phos}} F^{\text{Pi}} - k_{\text{rephos}} F^D - k_{\text{off},+}^D T_+^D - k_{\text{off},-}^D T_-^D, \quad (33)$$

$$\begin{aligned} \frac{dT_{\pm}^T}{dt} = & k_{\text{on},\pm}^T G^T (T_{\pm}^{\text{Pi}} + T_{\pm}^D) + (k_{\text{off},\pm}^{\text{Pi}} T_{\pm}^{\text{Pi}} + k_{\text{off},\pm}^D T_{\pm}^D) \eta_{\pm}^T - k_{\text{hyd}} T_{\pm}^T + k_{\text{rehyd}} T_{\pm}^{\text{Pi}} \\ & - k_{\text{off},\pm}^T T_{\pm}^T (\eta_{\pm}^{\text{Pi}} + \eta_{\pm}^D) - k_{\text{on},\pm}^D G^D T_{\pm}^T, \end{aligned} \quad (34)$$

$$\begin{aligned} \frac{dT_{\pm}^{\text{Pi}}}{dt} = & k_{\text{hyd}} T_{\pm}^T - k_{\text{rehyd}} T_{\pm}^{\text{Pi}} + (k_{\text{off},\pm}^T T_{\pm}^T + k_{\text{off},\pm}^D T_{\pm}^D) \eta_{\pm}^{\text{Pi}} - k_{\text{phos}} T_{\pm}^{\text{Pi}} + k_{\text{rephos}} T_{\pm}^D \\ & - k_{\text{off},\pm}^{\text{Pi}} T_{\pm}^{\text{Pi}} (\eta_{\pm}^T + \eta_{\pm}^D) - T_{\pm}^{\text{Pi}} (k_{\text{on},\pm}^T G^T + k_{\text{on},\pm}^D G^D), \end{aligned} \quad (35)$$

$$\begin{aligned} \frac{dT_{\pm}^D}{dt} = & k_{\text{on},\pm}^D G^D (T_{\pm}^T + T_{\pm}^{\text{Pi}}) + (k_{\text{off},\pm}^T T_{\pm}^T + k_{\text{off},\pm}^{\text{Pi}} T_{\pm}^{\text{Pi}}) \eta_{\pm}^D + k_{\text{phos}} T_{\pm}^{\text{Pi}} - k_{\text{rephos}} T_{\pm}^D \\ & - k_{\text{off},\pm}^D T_{\pm}^D (\eta_{\pm}^T + \eta_{\pm}^{\text{Pi}}) - k_{\text{on},\pm}^T G^T T_{\pm}^D, \end{aligned} \quad (36)$$

where

$$\eta_{\pm}^T = \frac{T_{\pm}^T}{N} \left(1 - \frac{T_{\pm}^{\text{Pi}}}{N} \right), \quad (37)$$

$$\eta_{\pm}^D = \frac{T_{\pm}^D}{N}, \quad (38)$$

$$\eta_{\pm}^{\text{Pi}} = 1 - \eta_{\pm}^T - \eta_{\pm}^D. \quad (39)$$

In table A1 we list the meaning and values of the rate constants used in our implementation of the BC model.

We note that the original equations in the +202/-+BC model did not include reversible reactions as shown here. This amounts to setting k_{renex} , k_{rehyd} , and k_{rephos} to 0 equations (29)–(36). The interpretation of η_j^i is the probability that the subunit adjacent to the j tip is in the i hydrolysis state. The equations of motion of these

Table A1. Rate constants in the BC model. The prefix ‘re’ indicates the reverse of a kinetically dominant forward reaction (i.e. nearly irreversible reactions). The value of rate constants for these reverse reactions is taken to be equal to the corresponding forward reaction rate multiplied by a small parameter ϵ . We typically take $\epsilon = 0.01$. Some of these reactions, such as the nucleotide exchange reaction, are second order reactions. For example the proper rate of reaction for conversion of G^D to G^T is $k_{\text{nex}}^*[G^D][\text{ATP}]$. We treat such cases as pseudo-first order reactions by assuming that the concentration of the species which we do not track is constant and that its concentration is contained in the rate constant used. Thus $k_{\text{nex}} = k_{\text{nex}}^*[\text{ATP}]$ in our model. This assumption of constant concentrations of free ATP, ADP, and Pi is reasonable in cellular environments. All values are taken from [20, 23].

Label	Reaction	Value
$k_{\text{on},+}^T$	Polymerization of G^T to barbed end	$11.6 \mu\text{M}^{-1} \text{s}^{-1}$
$k_{\text{on},-}^T$	Polymerization of G^T to pointed end	$1.3 \mu\text{M}^{-1} \text{s}^{-1}$
$k_{\text{off},+}^T$	Depolymerization of F^T from barbed end	1.4s^{-1}
$k_{\text{off},-}^T$	Depolymerization of F^T from pointed end	0.8s^{-1}
$k_{\text{on},+}^D$	Polymerization of G^D to barbed end	$2.9 \mu\text{M}^{-1} \text{s}^{-1}$
$k_{\text{on},-}^D$	Polymerization of G^D to pointed end	$0.13 \mu\text{M}^{-1} \text{s}^{-1}$
$k_{\text{off},+}^D$	Depolymerization of F^D from barbed end	5.4s^{-1}
$k_{\text{off},-}^D$	Depolymerization of F^D from pointed end	0.25s^{-1}
$k_{\text{off},+}^{\text{Pi}}$	Depolymerization of F^{Pi} from barbed end	1.4s^{-1}
$k_{\text{off},-}^{\text{Pi}}$	Depolymerization of F^{Pi} from pointed end	0.8s^{-1}
k_{hyd}	ATP hydrolysis converting F^T to F^{Pi}	0.3s^{-1}
k_{rehyd}	ATP condensation converting F^{Pi} to F^T	$\epsilon 0.3 \text{s}^{-1}$
k_{nex}	Nucleotide exchange converting G^D to G^T	0.01s^{-1}
k_{renex}	Nucleotide exchange converting G^T to G^D	$\epsilon 0.01 \text{s}^{-1}$
k_{phos}	Inorganic phosphate release converting F^{Pi} to F^D	0.002s^{-1}
k_{phos}	Inorganic phosphate capture converting F^D to F^{Pi}	$\epsilon 0.002 \text{s}^{-1}$

variables in principle depend on the hydrolysis state of the subunit next to them toward the center of the filament, and equations (29)–(36) represent the truncation of the resulting set of recursion equations. This is accomplished by assuming that η_j^i depends only on the tip subunit hydrolysis state through equations (34)–(36). These equations were arrived at by inspecting the time course of the η_j^i and the T_j^i variables and discerning the equations which approximately related the two. The system of equations (29)–(36) does not admit an analytical solution but can be numerically integrated with appropriate initial conditions specified [20].

We check the accuracy of the truncation assumption of the BC model by comparing a predicted time course to the results of a simulation using the software package Mechanochemical Dynamics of Active Networks (MEDYAN). MEDYAN was developed to perform coarse-grained simulations of active networks and combines stochastic chemical algorithms with detailed mechanics as well as coupling between reaction rates of force-sensitive chemical reactions and the mechanical state of the species involved [24]. In figures A1 and A2 we show the simulated time courses as well as the mean-field prediction of the BC model.

The steady-state vector \mathbf{x}^{ss} satisfying $\mathbf{f}(\mathbf{x}^{\text{ss}}) = \mathbf{0}$ can be found by numerically solving the root of the right hand sides of equations (29)–(36). Equations (29)–(33) sum to zero, reflecting the conservation of total actin M encoded in these reactions. Also each of the two sets of equations (34)–(36) sum to zero, reflecting the conservation of plus end tips and minus end tips. Thus the system $\dot{\mathbf{x}} = \mathbf{f}(\mathbf{x})$ represented by equations (29)–(36) is linearly dependent, and no solution to $\mathbf{f}(\mathbf{x}^{\text{ss}}) = 0$ exists unless we specify additional equations. These additional equations are

$$G^T + G^D + F^T + F^{\text{Pi}} + F^D = M, \quad (40)$$

$$T_{\pm}^T + T_{\pm}^{\text{Pi}} + T_{\pm}^D = N_{\pm}. \quad (41)$$

For unbranched filaments considered here, the number of plus end tips is equal to the number of minus end tips: $N_+ = N_- = N$. Solving $\mathbf{f}(\mathbf{x}^{\text{ss}}) = 0$ gives one solution for which all variables are nonnegative, so there is a unique realistic steady-state solution for a given set of parameters M and N . The eigenvalues of the BC Jacobian evaluated at the equilibrium point $\mathbf{J}^* = \frac{\partial \mathbf{f}}{\partial \mathbf{x}} \Big|_{\mathbf{x}=\mathbf{x}^{\text{ss}}}$ indicate the stability of the steady-state. 3 of the 11 eigenvalues are zero, corresponding to the 3 linear conservation laws in our system. This implies that the dynamics of the BC model lie on an 8-dimensional submanifold of the full 11-dimensional variable space, and this submanifold is determined by the parameters M and N . The remaining eigenvalues are negative, indicating that the unique nonnegative vector \mathbf{x}^{ss} is attracting and stable. We note that this equilibrium point of the dynamics actually corresponds to a non-equilibrium steady-state of the chemical system, since this state corresponds to actin

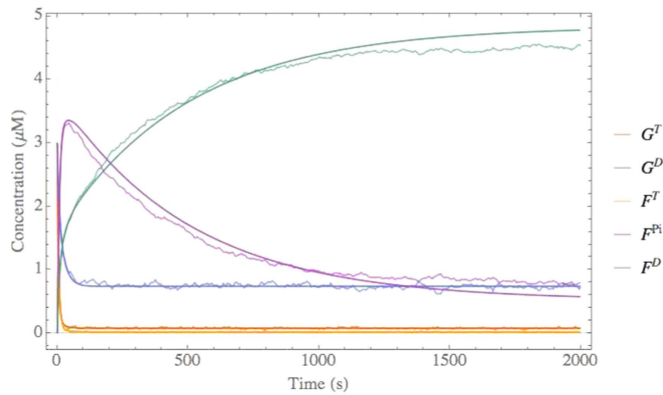


Figure A1. Time course of the concentrations of the various species following the addition of $3 \mu\text{M}$ of G^T and $3 \mu\text{M}$ of G^D actin to a bath with a number concentration $N = 0.017 \mu\text{M}$ of seed filaments. The mean-field BC (smooth curve) model accurately predicts the shape of the time-courses resulting from the stochastic simulation (noisy curve).

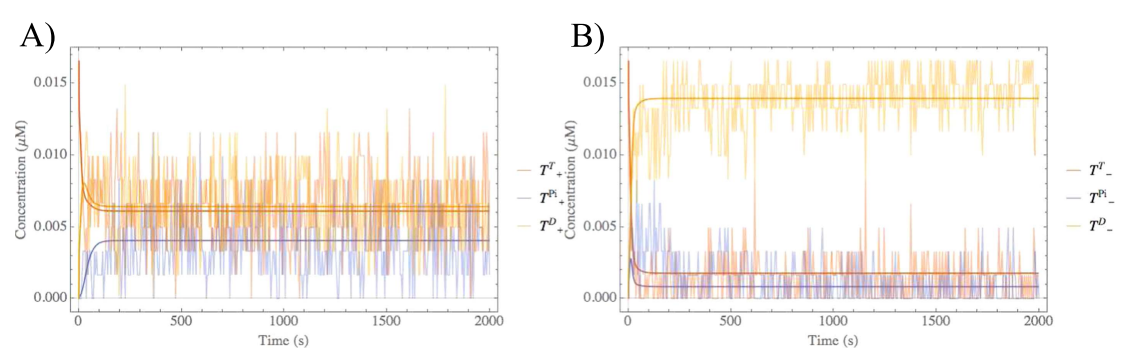


Figure A2. Time course of the concentrations of the various tip species at the plus (A) and minus (B) ends, following the addition of $3 \mu\text{M}$ of G^T and $3 \mu\text{M}$ of G^D actin to a bath with a number concentration $N = 0.017 \mu\text{M}$ of seed filaments. The noisiness of the stochastic trajectories results from the small copy number of filaments. Note how quickly these concentrations attain their steady-state values with this parameterization. This implies that not tracking these variables explicitly, as in the QSSA and CT models is valid for most of the trajectory.

treadmilling, fueled by ATP hydrolysis. This chemical driving is manifested in the values of certain pseudo-first order reaction rate constants such as k_{nex} .

Appendix B. Steady-state concentrations in the Brooks–Carlsson model

We show here that the independence of the steady-state concentrations of some species on M is also present in the BC model. We do this by consideration of the system of algebraic equations $\mathbf{f}(\mathbf{x}^{\text{ss}}) = \mathbf{0}$. The Jacobian matrix of system at the steady-state (see equation (24)) is effectively visualized in figure B1.

Now that we can grasp which species are coupled to which other species, we observe that no species depend on F^T , F^{Pi} , or F^D , except those species themselves. Therefore we could ignore the equations of motions of these variables and the resulting subsystem of equations would be closed. Now that subsystem will be linearly dependent, but we can supplement it with the following equations to make it independent:

$$T_{\pm}^T + T_{\pm}^{Pi} + T_{\pm}^D = N. \quad (42)$$

The subsystem of equations could now be solved, giving the steady-state concentrations of all species except for F^T , F^{Pi} , and F^D . M , the total amount of actin, does not enter into any of the equations of the subsystem, and so the solution of that system does not depend on M . Therefore, the steady-state concentration of each species except F^T , F^{Pi} , and F^D does not depend on the initial conditions, however they do depend on the parameter N .

Now we consider the case where $\epsilon = 0$. Referring to figure B1, we see that this would mean that no species depends on F^D . By reasoning similar to the above, this implies that the steady-state concentration of each species except F^D could be determined without specifying M . Thus, the steady-state concentration of only F^D depends on the initial conditions in this case.

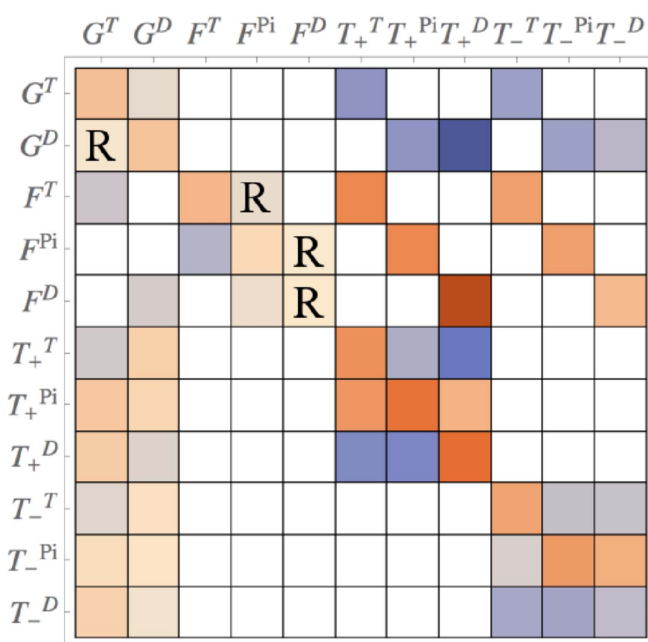


Figure B1. Visualization of J^* to understand the couplings in the BC model. If $\frac{\partial x_i}{\partial x_j} \neq 0$, then J_{ij}^* will be nonzero. If this coupling causes x_i to increase, the entry in the matrix is colored blue, and if it causes x_i to decrease, the entry is red. The saturation of the color indicates the magnitude of the coupling. An 'R' is placed in the plot if that element is nonzero only due to the inclusion of slow reversible reactions, i.e. when $\epsilon > 0$. The corresponding plot for the CT model is identical to the top left 5 by 5 matrix in this plot.

ORCID iDs

Carlos Floyd <https://orcid.org/0000-0002-6270-7250>

Christopher Jarzynski <https://orcid.org/0000-0002-3464-2920>

Garegin Papoian <https://orcid.org/0000-0001-8580-3790>

References

- [1] Lodish H, Baltimore D, Berk A, Zipursky S L, Matsudaira P and Darnell J 1995 *Molecular Cell Biology* vol 3 (New York: Scientific American Books)
- [2] Theriot J A and Mitchison T J 1991 Actin microfilament dynamics in locomoting cells *Nature* **352** 126
- [3] Schmidt A and Hall M N 1998 Signaling to the actin cytoskeleton *Annu. Rev. Cell Dev. Biol.* **14** 305–38
- [4] Vogel V and Sheetz M 2006 Local force and geometry sensing regulate cell functions *Nat. Rev. Mol. Cell Biol.* **7** 265–75
- [5] Carlier M-F, Laurent V, Santolini J, Melki R, Didry D, Xia G-X, Hong Y, Chua N-H and Pantaloni D 1997 Actin depolymerizing factor (ADF/cofilin) enhances the rate of filament turnover: implication in actin-based motility *J. Cell Biol.* **136** 1307–22
- [6] Pollard T D 1986 Rate constants for the reactions of ATP- and ADP-actin with the ends of actin filaments *J. Cell Biol.* **103** 2747–54
- [7] Andrianantoandro E and Pollard T D 2006 Mechanism of actin filament turnover by severing and nucleation at different concentrations of ADF/cofilin *Mol. Cell* **24** 13–23
- [8] Isambert H, Venier P, Maggs A C, Fattoum A, Kassab R, Pantaloni D and Carlier M-F 1995 Flexibility of actin filaments derived from thermal fluctuations. Effect of bound nucleotide, phalloidin, and muscle regulatory proteins *J. Biol. Chem.* **270** 11437–44
- [9] Wegner A and Engel J 1975 Kinetics of the cooperative association of actin to actin filament *Biophys. Chem.* **3** 215–25
- [10] Cooke R 1975 Role of the bound nucleotide in the polymerization of actin *Biochemistry* **14** 3250–6
- [11] Wegner A 1976 Head to tail polymerization of actin *J. Mol. Biol.* **108** 139–50
- [12] Pantaloni D, Hill T L, Carlier M-F and Korn E D 1985 A model for actin polymerization and the kinetic effects of ATP hydrolysis *Proc. Natl Acad. Sci.* **82** 7207–11
- [13] Hill T L and Kirschner M W 1982 Subunit treadmilling of microtubules or actin in the presence of cellular barriers: possible conversion of chemical free energy into mechanical work *Proc. Natl Acad. Sci.* **79** 490–4
- [14] Korn E D, Carlier M-F and Pantaloni D 1987 Actin polymerization and ATP hydrolysis *Science* **238** 638–45
- [15] Dufort P A and Lumsden C J 1996 How profilin/barbed-end synergy controls actin polymerization: a kinetic model of the ATP hydrolysis circuit *Cell Motility Cytoskeleton* **35** 309–30
- [16] Bindschadler M, Osborn E A, Dewey C F and McGrath J L 2004 A mechanistic model of the actin cycle *Biophys. J.* **86** 2720–39
- [17] Li X, Kierfeld J and Lipowsky R 2009 Actin polymerization and depolymerization coupled to cooperative hydrolysis *Phys. Rev. Lett.* **103** 048102
- [18] Stukalin E B and Kolomeisky A B 2006 Atp hydrolysis stimulates large length fluctuations in single actin filaments *Biophys. J.* **90** 2673–85
- [19] Yarmola E G, Dranishnikov D A and Bubb M R 2008 Effect of profilin on actin critical concentration: a theoretical analysis *Biophys. J.* **95** 5544–73
- [20] Brooks F J and Carlsson A E 2009 Nonequilibrium actin polymerization treated by a truncated rate-equation method *Phys. Rev. E* **79** 031914

- [21] Brooks F J and Carlsson A E 2008 Actin polymerization overshoots and ATP hydrolysis as assayed by pyrene fluorescence *Biophys. J.* **95** 1050–62
- [22] Campbell S L, Meyer C D Jr and Rose N J 1976 Applications of the drasin inverse to linear systems of differential equations with singular constant coefficients *SIAM J. Appl. Math.* **31** 411–25
- [23] Fujiwara I, Vavylonis D and Pollard T D 2007 Polymerization kinetics of ADP- and ADP-Pi-actin determined by fluorescence microscopy *Proc. Natl Acad. Sci.* **104** 8827–32
- [24] Popov K, Komianos J and Papoian G A 2016 Medyan: mechanochemical simulations of contraction and polarity alignment in actomyosin networks *PLoS Comput. Biol.* **12** e1004877